CLINICAL STUDY

CrossMark

Non-invasive genotype prediction of chromosome 1p/19q co-deletion by development and validation of an MRI-based radiomics signature in lower-grade gliomas

Yuqi Han[1,2,4] · Zhen Xie[3] · Yali Zang[2,4,8] · Shuaitong Zhang[2,4,8] · Dongsheng Gu[2,4,8] · Mu Zhou[5] · Olivier Gevaert[5] · Jingwei Wei[2,4,8] · Chao Li[3] · Hongyan Chen[6] · Jiang Du[6] · Zhenyu Liu[2,4,8] · Di Dong[2,4,8] · Jie Tian[2,4,7,8] · Dabiao Zhou[3,9]

Abstract

Purpose To perform radiomics analysis for non-invasively predicting chromosome 1p/19q co-deletion in World Health Organization grade II and III (lower-grade) gliomas.

Methods This retrospective study included 277 patients histopathologically diagnosed with lower-grade glioma. Clinical parameters were recorded for each patient. We performed a radiomics analysis by extracting 647 MRI-based features and applied the random forest algorithm to generate a radiomics signature for predicting 1p/19q co-deletion in the training cohort (n = 184). The clinical model consisted of pertinent clinical factors, and was built using a logistic regression algorithm. A combined model, incorporating both the radiomics signature and related clinical factors, was also constructed. The receiver operating characteristics curve was used to evaluate the predictive performance. We further validated the predictability of the three developed models using a time-independent validation cohort (n = 93).

Results The radiomics signature was constructed as an independent predictor for differentiating 1p/19q co-deletion genotypes, which demonstrated superior performance on both the training and validation cohorts with areas under curve (AUCs) of 0.887 and 0.760, respectively. These results outperformed the clinical model (AUCs of 0.580 and 0.627 on training and validation cohorts). The AUCs of the combined model were 0.885 and 0.753 on training and validation cohorts, respectively, which indicated that clinical factors did not present additional improvement for the prediction.

Conclusion Our study highlighted that an MRI-based radiomics signature can effectively identify the 1p/19q co-deletion in histopathologically diagnosed lower-grade gliomas, thereby offering the potential to facilitate non-invasive molecular subtype prediction of gliomas.

Keywords Lower-grade glioma · 1p/19q Co-deletion · Prediction · Radiomics · Magnetic resonance imaging

---

Yuqi Han, Zhen Xie and Yali Zang have contributed equally to this work. Di Dong, Jie Tian, and Dabiao Zhou are the corresponding authors.

✉ Di Dong
   di.dong@ia.ac.cn

✉ Jie Tian
   tian@ieee.org

✉ Dabiao Zhou
   dabiaozhou@163.com

Extended author information available on the last page of the article

Introduction

Gliomas are the most common and highly malignant primary brain tumors in adults. Diffuse lower-grade gliomas, comprising astrocytomas, oligodendrogliomas and mixed oligoastrocytomas of World Health Organization (WHO II and III grade), pose a great challenge both in histopathological classification and clinical treatment [1–3]. Astroglial and oligodendroglial tumors are believed to share a common neural/tumor precursor cell, but lower-grade gliomas display high molecular heterogeneity generated from different genetic events during cell differentiation and tumor development [2–6]. Currently, molecular profiling clarifies the oligodendroglial characteristics of glioma by chromosome arm 1p and 19q co-deletion [2–4, 7], which was included

as a genetic determinant for the subtype nomenclature of gliomas in the latest (2016) WHO classification of tumors of the central nervous system [2]. Chromosome 1p and 19q co-deletion has proven to be a beneficial prognostic factor due to a favorable response to chemo/radiotherapy [8–11]. However, the 1p/19q co-deletion genotype is currently examined via fluorescence in situ hybridization (FISH) or polymerase chain reaction (PCR) [12]; both invasive biopsy-based approaches carry a high risk of neurological deficit and morbidity, especially for patients with an eloquent mass [13, 14]. Therefore, the development of a noninvasive method capable of accurately detecting the 1p/19q co-deletion genotype prior to surgery is of great clinical significance and may improve individualized treatment decisions.

Histopathological diagnosis of lower-grade glioma has considerable uncertainty in distinguishing astrocytomas, oligodendrogliomas and oligoastrocytomas due to the morphological continuum on a microscopic scale and the absence of reliable immunohistochemical markers. However, molecular genetics could uncover the underlying biological characteristics of lower-grade gliomas which leads to the differences of clinical presentation, radiological features and treatment responses among molecular subgroups. Microarray analysis showed that the gene expression profile of oligodendrogliomas with 1p19q co-deletion was partially similar to the expression profile of normal brain samples [15, 16]. This supported the hypothesis that the cell of origin for gliomas with 1p19q co-deletion could grow into both oligodendrocytes and neurons, be a bi-potential progenitor cell [15]. Indeed, infiltrative growth was more common in tumors with intact 1p19q and indistinct, irregular borders were more likely to have a 1p19q co-deletion [17, 18]. Prior image-based studies suggested that the radiological characteristics of gliomas, including an indistinct tumor border and heterogeneous intensity signal observed with MRI, were correlated with a 1p/19q co-deletion status of gliomas [19–21]. However, these qualitative image features suffer from inter-observer variability and fail to provide precise measurements for diagnosis. Radiomics is an emerging field of cancer research that noninvasively assesses cancer biology through quantitative imaging analysis [22–26]. The validity of radiomic features has been successfully verified in lung, head, neck and colorectal cancer [27–29] among others. With respect to gliomas, MRI is a routine diagnostic tool that characterizes detailed biological information about the tumor [30]. However, the feasibility of using MRI-based radiomics for 1p19q co-deletion genotype prediction has not been explicitly addressed.

By developing and validating an MRI-based radiomics signature, we aim to identify the 1p/19q co-deletion genotype from the histopathological phenotype of lower-grade gliomas, and verify the radiomics method which can noninvasively predict the molecular subtype of gliomas.

Methods

Study cohort

This retrospective study was approved and carried out with consent from the appropriate institutional ethics committee. The cohort included 277 patients with primary lower-grade (WHO grade II and III) gliomas who underwent surgery between January 2012 and June 2016. The requirement for informed consent was waived due to the retrospective nature of the study and all patients were de-identified. Patient inclusion criteria for our analysis were as follows: (a) histopathologically confirmed astrocytomas, oligodendrogliomas and oligoastrocytomas (WHO grade II and III), and molecular subtypes determined as 1p/19q co-deletion and non-co-deletion according to the WHO 2016 diagnostic criteria, (b) tumor not treated with any advanced treatments at initial diagnosis including biopsy testing, radio/chemotherapy or surgery, and (c) conventional MRI examination within 4 weeks prior to surgery. The cohort was divided into a training cohort of 184 patients collected from January 2012 to December 2014 and a time-independent validation cohort of 93 patients collected from January 2015 to June 2016.

FISH examination of chromosome 1p/19q

Dual-color FISH hybridizations were performed using locus specific identifier (LSI) probe sets 1p36/1q25 and 19q13/19p13 (Abbot Laboratories, Lake Bluff, IL, USA). For all tumor samples, nuclei were counterstained with 4′,6-diamidino-2-phenylindole (DAPI). The assay was evaluated using a fluorescence microscope (Olympus BX51 TRF, Olympus Corp., Shinjuku, Tokyo, Japan) as per the manufacturer's instructions. Fluorescent signals from at least 100 non-overlapping nuclei were enumerated for each probe. The assessment was consensus-classified by two pathologists with 23 and 25 years of experience, respectively.

Image data acquisition

MRI examinations were performed on a 3.0 T scanner (MAGNETTOM Trio, Siemens Healthcare GmbH, Erlangen, Germany) using an eight-channel phase array coil. Scanning parameters [repetition time (TR), echo time (TE), field of view (FOV), and flip angle (FA)] were as follows: T2-weighted imaging (T2WI) with TR 4500 ms/TE 84 ms, FOV = 220 mm × 186 mm, resolution = 384 × 259, and FA = 120°. Slice thickness and slice interval were 5.0
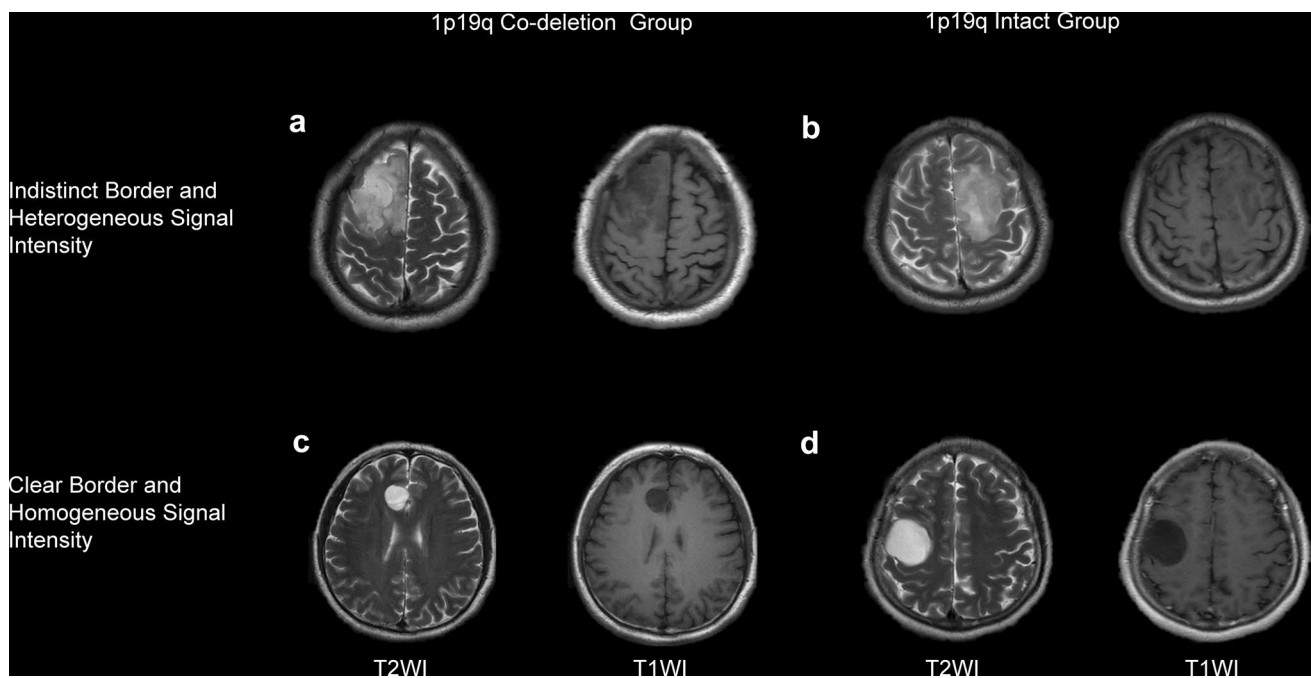
Fig. 1 The representative cases of lower-grade glioma associated with the 1p/19q intact and co-deletion in T2WI and T1WI. Note: For 1p19q co-deletion group, the patient usually exhibits indistinct border and heterogeneous signal intensity (patient **a**); but, some patients will exhibit a misleading phenotype (patient **c**); for 1p19q intact group, the patient usually exhibits clear border and homogeneous signal intensity (patient **d**); but, some patients will exhibit a misleading phenotype (patient **b**). For patient **b** and **c**, the proposed radiomics signature successfully predicted their 1p19q genotype

and 1.5 mm, respectively for all axial sequences. The representative images of the 1p/19q co-deletion and intact groups are shown in Fig. 1.

Region of interest segmentation

Manual tumor segmentation was individually performed by two certified neurosurgeons with 15 years of neuro-oncology experience. The region-of-interest (ROI) was delineated on two-dimensional T2-weighted images covering the peripheral edema area using the ITK-SNAP software (http://www.itksnap.org/pmwiki/pmwiki.php) [31]; the overlapped area from their annotations was selected as the final ROI. We tested the variability of radiomic features extracted from the ROI regions that were delineated by the two neurosurgeons separately using inter-observer correlation coefficients (ICCs). The agreement among radiomic features ranged from 0.75 to 0.99.

Radiomic feature extraction

We developed an analytical platform to extract three different types of radiomic features from images including 25 non-textural, 54 textural and wavelet features. Non-textural features and wavelet features measured tumor shape, size and intensity. Textural features described the intrinsic

heterogeneous texture of the tumor lesions based on four textural matrices: the gray level co-occurrence matrix (GLCM) [32], the gray level run-length matrix (GLRLM) [33–36], the gray level size zone matrix (GLSZM) [36], and the neighborhood gray-tone difference matrix (NGTDM) [37]. Before constructing these matrices, we discretized the MRI ROI by resampling the voxel intensities into equally spaced bins. This discretization step reduced image noise and normalized pixel intensities across all patients. Finally, we adopted wavelet transformation to capture the features from different scales in low and high frequencies. We applied a three-dimensional wavelet transformation for each patient data, which deconstructs the original image set in to eight filtered image sets in three directions. Finally, we extracted 647 radiomic features consisting of shape and size features (8), first order statistics features (17), textural features (54) for the original image set, and first order statistics and textural features for 8 wavelet filtered image sets $[(17 + 54) \times 8]$. A complete description of the calculated radiomic features is provided in the Supporting Information (S1).

Feature reduction and radiomics signature construction

VarianceThreshold was applied to exclude the features with low variance on the training cohort, and the parameter was

set to "threshold $= 0.8 \times (1-0.8)$". We then used univariate analysis with p-values less than 0.1 to reduce the dimensionality of the radiomic features and select the discriminative features on the training cohort. We applied the random forest algorithm to generate a radiomics signature for prediction of the 1p/19q co-deletion genotype. The algorithm was implemented based on the selected radiomic features and the 1p/19q co-deletion genotype. When implementing the random forest algorithm, three parameters were tuned on the training cohort: (a) the number of decision trees, (b) the maximum depth of the trees and (c) the minimum sample of the leaf, along with five-fold cross validation. The random forest algorithm was implemented using the Python, version 2.7.14 "scikit-learn" package.

Clinical and combined model construction

The clinical model consisted of related clinical factors and radiological traits using a logistic regression model. Clinical factors are given in Table 1 [38]. Furthermore, two main radiological characteristics, tumor border and signal intensity [19], were also included and scored (as 0 or 1: indistinct vs. sharp, heterogeneous vs. homogeneous, respectively) on T2-weighted images by two neuro-radiologists with 10 years of experience. Univariate analysis was used for selection of the effective variables, with p-values < 0.1. The combined model integrated both the radiomics signature and final selected clinical and radiological factors using logistic regression modeling.

Model comparison

For model comparisons, we used the Delong tests [39] to determine significant difference among to the areas under curve (AUCs). A p-value < 0.05 was considered as indicative of additional improvement of the developed radiomics signature. Indexes including AUC, prediction accuracy, sensitivity and specificity were calculated for all models.

Statistical analysis

We used the Mann–Whitney *U* test to analyze patients' baseline characteristics and determine the statistical difference of the radiomics signature of the 1p/19q co-deletion and non-co-deletion groups, and p-values < 0.05 were considered statistically significant. Receiver operating characteristics (ROC) curve analyses were performed to illustrate the predictive performance of the three proposed models and AUC was calculated for both the training and validation cohorts. We adopted the cut-off value on the training cohort and applied the training cut-off value into the validation cohort to obtain the accuracy, sensitivity and specificity. We performed statistical analysis using IBM SPSS Statistics,

Version 22.0. Categorical variables were presented as numbers or percentages and continuous variables were expressed as medians.

Results

Patient characteristics

The demographic information of the patient cohorts is given in Table 1. The cohort contained 171 males and 106 females, and mean age was 42.29 years (range, 18–76 years). A total of 109 (39%) patient exhibited 1p/19q co-deletion and 168 (61%) patients did not. The cohort was divided into a training cohort of 184 patients and a time-independent validation cohort of 93 patients. There were no statistical differences in demographic or clinical characteristics between the training and validation cohorts (p = 0.065 to p = 0.941).

MRI features and radiomics signature construction

We extracted 647 radiomic features from each patient's imaging. A total of 64 radiomic features were selected after excluding redundant features. Detailed information of the selected 64 features is given in the Supporting Information (S2). Random forest algorithms, formulated the radiomics signature, where the number of decision trees was set to 150, and the maximum depth of the trees was set to 4, minimum sample of the leaf was 12 in our final model. The selected 64 features for constructing the radiomics signature are listed in the Supporting Information (S2). The radiomics signature for each patient, divided by training and validation cohorts is shown in Fig. 2a, b.

1p/19q genotype prediction

The radiomics signature could discriminate between the 1p/19q co-deletion and non-co-deletion groups, with significant differences on both the training (p < 0.001) and validation cohorts (p < 0.001) (see Supporting Information S3). The radiomics signature presented appealing performance with AUCs of 0.887 and 0.760 on training and validation cohorts, respectively (Fig. 3). Boxplots for the radiomics signature divided by 1p/19q co-deletion and non-co-deletion groups are shown in Fig. 2c–d. For stratification analysis, the radiomics signature still demonstrated satisfactory performance when adjusting for sex, age and grade (see Supporting Information S3).

Distinct signal intensity was selected as an additional predictor of 1p/19q co-deletion after univariate analysis (see Supporting Information S4). The clinical model achieved AUCs of 0.580 and 0.627 on the training and validation cohorts, respectively (Fig. 3). The predictive

Table 1 Clinical characteristics of patients with lower-grade glioma (n = 277)

Characteristic	Training cohort (n = 184)	Validation cohort (n = 93)	Whole cohort (n = 277)	p-value
Age (years, mean [range])	41.67 (18–66)	43.53 (22–76)	42.29 (18–76)	0.183
Sex (n [%])				0.093
Male	120 (0.65)	51 (0.55)	171 (0.62)	
Female	64 (0.35)	42 (0.45)	106 (0.38)	
Pre-operative epilepsy (n [%])				0.347
Yes	82 (0.45)	47 (0.51)	129 (0.47)	
No	102 (0.55)	46 (0.49)	148 (0.53)	
Border Clearness (n [%])				
Yes	102 (0.55)	47 (0.51)	149 (0.54)	0.440
No	82 (0.45)	46 (0.49)	128 (0.46)	
Homogeneity (n [%])				
Yes	32 (0.17)	20 (0.22)	52 (0.19)	0.408
No	152 (0.83)	73 (0.78)	225 (0.81)	
Enhance (n [%])				
Yes	124 (0.67)	57 (0.61)	177 (0.68)	0.314
No	60 (0.33)	36 (0.39)	85 (0.32)	
Bleeding (n [%])				
Yes	14 (0.08)	2 (0.02)	16 (0.06)	0.066
No	170 (0.92)	91 (0.98)	261 (0.94)	
Edema (n [%])				
No edema	29 (0.16)	15 (0.16)	37 (0.16)	0.941
Mild edema	112 (0.61)	58 (0.62)	165 (0.61)	
Moderate edema	43 (0.23)	20 (0.22)	60 (0.23)	
Cystic formation (n [%])				
Yes	66 (0.36)	28 (0.30)	94 (0.34)	0.339
No	118 (0.64)	65 (0.70)	183 (0.66)	
WHO grade (n [%])				0.065
Grade II	114 (0.62)	68 (0.73)	182 (0.66)	
Grade III	70 (0.38)	25 (0.27)	95 (0.34)	
Left (n [%])				
No	104 (0.57)	53 (0.57)	157 (0.57)	0.941
Yes	80 (0.43)	40 (0.43)	120 (0.43)	
Right (n [%])				
No	83 (0.45)	43 (0.46)	126 (0.45)	0.859
Yes	101 (0.55)	50 (0.54)	151 (0.56)	
Both (n [%])				
No	3 (0.02)	3 (0.03)	6 (0.02)	0.389
Yes	181 (0.98)	90 (0.97)	271 (0.98)	
1p and 19q status (n [%])				0.251
Co-deletion	68 (0.37)	41 (0.44)	109 (0.42)	
Non-co-deletion	116 (0.63)	52 (0.55)	168 (0.61)	

$p < 0.05$ indicates a significant difference in patients' characteristics between the training and validation cohorts. Left, right and both represent the location of tumor in the brain

performance of the combined model improved when integrating the radiomics signature along with clinical factors (AUCs: 0.885 and 0.753). The Delong test revealed significant differences between the radiomics signature and the clinical model on both the training and validation cohorts ($p < 0.001$ and $p = 0.005$, respectively, Table 2), and significant differences between the combined model and the clinical model on both the training and validation cohorts ($p < 0.001$ and $p = 0.012$, respectively, Table 2). Among all of the models, the radiomics signature yielded
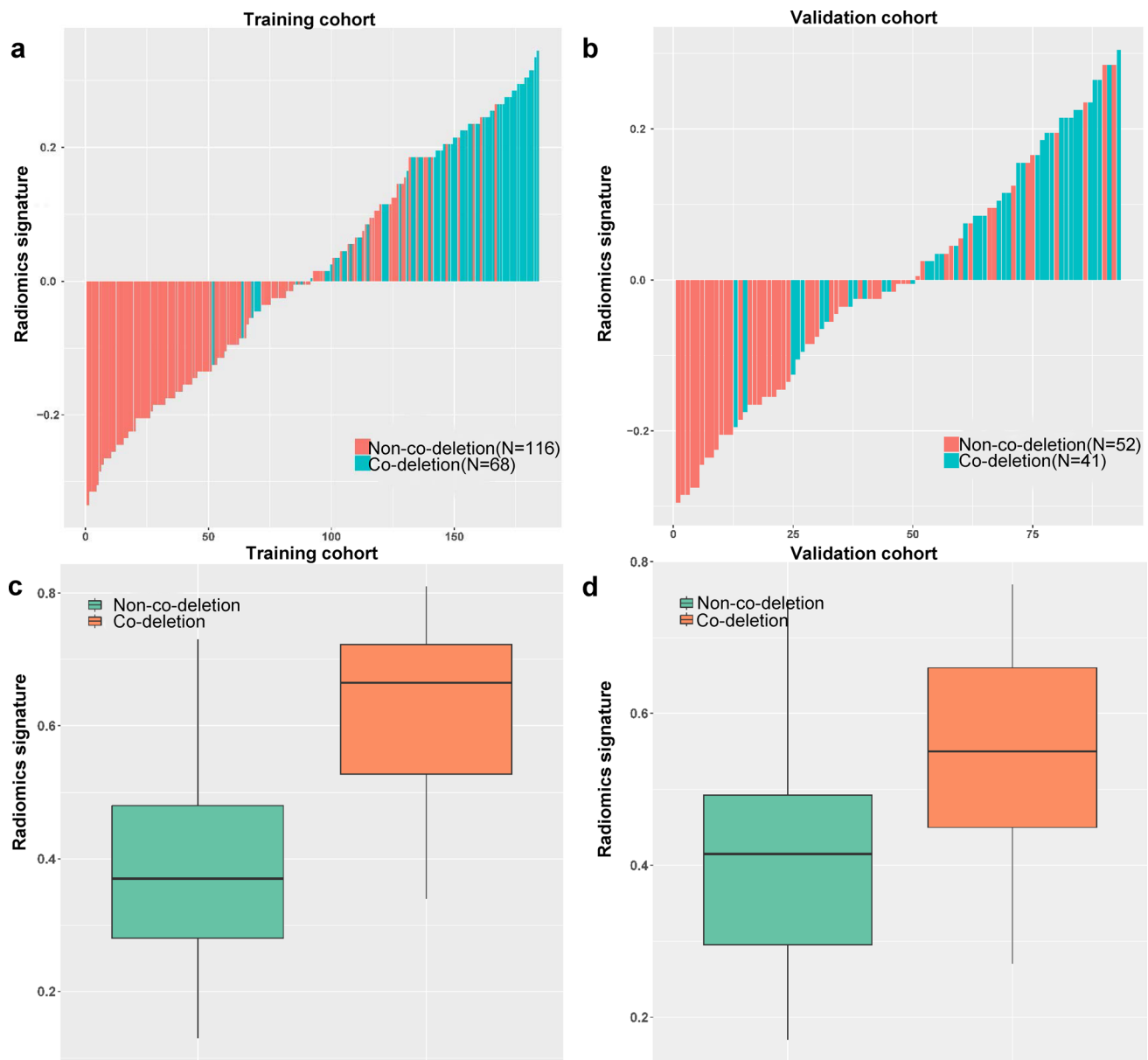
Fig. 2 The predictive performance of radiomics signature. **a** and **b** The barplots for the training cohort and the validation cohort with the radiomics signature for each patient; **c** and **d** The boxplots for radi-omics signature in training and validation cohorts, categorized by 1p/19q co-deletion and non-co-deletion groups for radiomics model

the highest AUC, and showed the best predictive performance for 1p/19q genotype.

Discussion

In this study, we applied the random forest algorithm to generate an MRI-based radiomics signature for the discrimination of a 1p/19q co-deletion genotype in histopathologically diagnosed lower-grade gliomas. The radiomics signature had

satisfactory performance for genotype prediction in both training and time-independent validation cohorts.

Maximal safe surgical resection is advocated as the standard of care of suspected lower-grade glioma patients [40, 41]. Both clinical and molecular factors, including IDH and 1p19q status, should be taken into account in surgical decision-making. The loss of heterozygosity of chromosome arm 1p and 19q is highly correlated with a positive response to radio/chemotherapy, indicating a preferable prognosis [2, 4, 9, 11, 42]. A recent study verified that gross-total resection was not related with improved survival of patients with
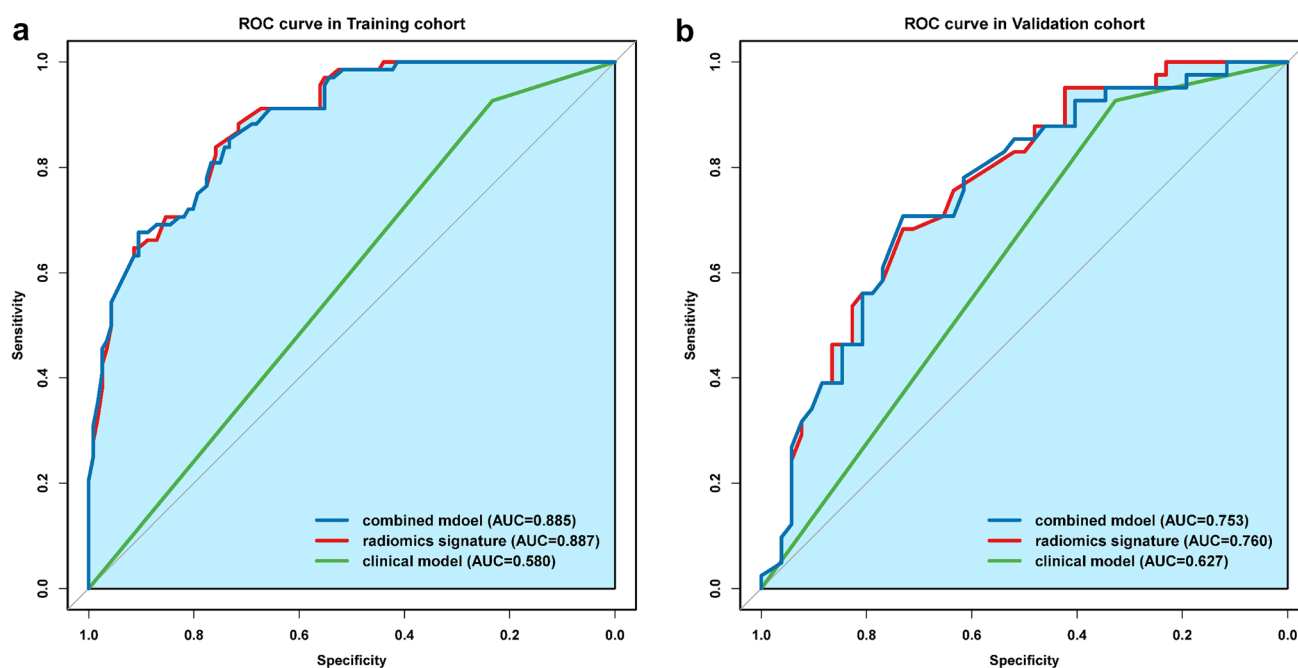
Fig. 3 The receiving operating characteristics (ROC) curves of the radiomics signature-based model, the clinical model and the combined model on the **a** training cohort and **b** validation cohort

Table 2 Diagnostic performance of the three proposed models

Different models	Training cohort (n = 184)				Validation cohort (n = 93)			
	SEN (%)	SPE (%)	ACC (%)	AUC (95% CI)	SEN (%)	SPE (%)	ACC (%)	AUC (95% CI)
Clinical	92.6	23.3	48.9	0.580 (0.530–0.629)	92.7	32.7	59.4	0.627 (0.551–0.703)
Radiomics	88.2	71.6	77.8	0.887 (0.841–0.933)	68.3	71.2	70.0	0.760 (0.663–0.857)
Combined	85.3	73.3	77.2	0.885 (0.839–0.932)	70.7	73.1	72.0	0.753 (0.654–0.852)

95% *CI* 95% confidence interval, *AUC* area under curve, *SEN* sensitivity, *SPE* specificity, *ACC* accuracy

chemosensitive oligodendroglioma through SEER-based analysis combined with a review of literature [43]. Van den Bent et al. suggested that the best factor that can benefit from chemotherapy predicts remains to be established in lower-grade glioma [17]. Due to the potential adverse effects of surgery, a wait-and-see policy was recommended among patients with suspected low-grade glioma and an expected favorable prognosis [17]. This clinical evidence manifested that knowledge of 1p and 19q status could help with appropriate surgical planning or aggressiveness. Accordingly, the noninvasive detection of 1p/19q co-deletion using medical imaging (routinely obtained before surgery), as opposed to tumor tissue sampling, could facilitate glioma molecular subtype identification and impact individualized treatment decisions.

We extracted 647 high-throughput quantitative imaging features from the T2-weighted images of each patient. A set of 64 radiomic features was selected using *VarianceThreshold* and univariate analysis before the random

forest algorithm was used. Of all 64 features, there were 26 intensity features and 38 textural features. The top three features for constructing the random forest model were ori_fos_skewness, Coif5_glcm_covariance and Coif2_glcm_sum_variance (see Supporting Information S2). The feature ori_fos_skewness measures the symmetry of the distribution of gray values in the original image, and reveals the degree of distortion for the image. The feature Coif5_glcm_covariance reveals the variability of gray values of the pixel pairs, and is a measurement of heterogeneity in an image filtered with low-pass in the x-direction and high-pass in the y- and z-direction. The feature Coif2_glcm_sum_variance reflects the change frequency and period of the texture in an image filtered with low-pass in the x- and y-direction and high-pass in the z-direction [44]. Particularly, the wavelet transformation decoupled image information by deconstructing the original images in low and high frequencies and reflecting detailed imaging characteristics. The image filtered with high-pass can describe the details and edges of the image,

and the image filtered with low-pass can exhibit the overall distribution of gray values in the image. The identified wavelet features showed that the spectral frequencies applied in wavelet transformation were informative for identifying 1p/19q co-deletion in gliomas, in concordance with a previous study [45].

To evaluate the performance of radiomics signature for predicting the 1p/19q co-deletion genotype, we additionally constructed two models: the clinical model and the combined model. Of all these models, the radiomics signature achieved the best performance. When the clinic-radiological information was incorporated with the radiomics signature, there were no differences between the combined model and the radiomics signature. But, the combined model exhibited far better performance than that of the clinical model, which means the radiomics signature, had strong predictive power for 1p/19q co-deletion. The explanation of such finding may be ascribed to the fact that the radiomics signature is built upon computerized algorithms to allow quantitative and objective assessment of tumor imaging data. By contrast, the heterogeneous signal intensity is performed by the subjective evaluation from the physicians, which has a large inter-observer variability.

Image quality and precise segmentation of tumor lesions are crucial for radiomics analysis. In this study, we imposed a full delineation on the lesion covering both the tumor parenchyma and infiltrating area of the tumor-brain interface, which guaranteed characterization of the radiomics algorithms with comprehensive intra-tumoral heterogeneity. We performed radiomics analysis on T2-weighted images since they are routinely used in clinical assessment of lower-grade glioma and especially T2-weighted images display hyper intense signals in lower-grade gliomas, allowing for a more accurate delineation of the tumor border compared to T1-weighted images [46].

Our study has several limitations. Firstly, this is a retrospective study that performed a time-independent validation with the data collected from a single center; multi-center data will be needed to allow external validation. Secondly, other MR sequences including T2 fluid attenuated inversion recovery (T2-FLAIR) sequence and diffusion weighted images (DWI) may provide extra functional and biological information; therefore, we recommend that future work includes more imaging modalities to explore the predictive power of radiomic features. Finally, our work is only focused on the prediction of the 1p/19q co-deletion genotype of lower-grade glioma, the analysis of additional molecular markers, including IDH1/2, ATRX, and TERT, will enable more comprehensive understanding of imaging-to-molecular associations of astrocytic and oligodendroglial lineage gliomas in the future.

In conclusion, our study highlighted that radiomic features can be used to pre-operatively and non-invasively distinguish the 1p/19q co-deletion genotype in patients with lower-grade gliomas. The radiomics signature displays appealing predictive performance, thereby offering the potential to identify the molecular subtype of gliomas noninvasively.

Disclaimer The content is solely the responsibility of the authors and does not necessarily represent the official views of the National Institutes of Health.

Compliance with ethical standards

Conflict of interest The authors declare that they have no conflicts of interest.

References

1. Chen B, Liang T, Yang P et al (2016) Classifying lower grade glioma cases according to whole genome gene expression. Oncotarget 7(45):74031–74042
2. Louis DN, Perry A, Reifenberger G et al (2016) The 2016 World Health Organization classification of tumors of the central nervous system: a summary. Acta Neuropathol 131:803–820
3. Network CGAR (2015) Comprehensive, integrative genomic analysis of diffuse low-grade gliomas. N Engl J Med 372:2481–2498
4. Smith JS, Perry A, Borell TJ et al (2000) Alterations of chromosome arms 1p Fand 19q as predictors of survival in oligodendrogliomas, astrocytomas, and mixed oligoastrocytomas. J Clin Oncol 18:636–636
5. Lindberg N, Jiang Y, Xie Y et al (2013) Oncogenic signaling is dominant to cell of origin and dictates astrocytic or oligodendroglial tumor development from oligodendrocyte precursor cells. J Neurosci 33(42):16805–16817
6. Appin CL, Brat DJ (2014) Molecular genetics of gliomas. Cancer J 20(1):66
7. Bauman G, Ino Y, Ueki K et al (2000) Allelic loss of chromosome 1p and radiotherapy plus chemotherapy in patients with oligodendrogliomas. Int J Radiat Oncol Biol Phys 48:825–830
8. Ino Y, Betensky RA, Zlatescu MC et al (2001) Molecular subtypes of anaplastic oligodendroglioma. Clin Cancer Res 7:839–845
9. Kaloshi G, Benouaich-Amiel A, Diakite F et al (2007) Temozolomide for low-grade gliomas predictive impact of 1p/19q loss on response and outcome. Neurology 68:1831–1836
10. Reifenberger J, Reifenberger G, Liu L et al (1994) Molecular genetic analysis of oligodendroglial tumors shows preferential allelic deletions on 19q and 1p. Am J Pathol 145:1175–1190
11. Theeler BJ, Yung WA, Fuller GN et al (2012) Moving toward molecular classification of diffuse gliomas in adults. Neurology 79:1917–1926

12. Woehrer A, Hainfellner JA (2015) Molecular diagnostics: techniques and recommendations for 1p/19q assessment. CNS Oncol 4:295–306

13. Sanai N, Martino J, Berger MS (2012) Morbidity profile following aggressive resection of parietal lobe gliomas: clinical article. J Neurosurg 116:1182–1186

14. Tate MC, Kim C-Y, Chang EF et al (2011) Assessment of morbidity following resection of cingulate gyrus gliomas: clinical article. J Neurosurg 114:640–647

15. Ducray F, Idbaih A, Reyniès AD et al (2008) Anaplastic oligodendrogliomas with 1p19q codeletion have a proneural gene expression profile. Mol Cancer 7(1):41

16. Mukasa A, Ueki K, Ge X et al (2010) Selective expression of a subset of neuronal genes in oligodendroglioma with chromosome 1p loss. Brain Pathol 14(1):34–42

17. Van den Bent MJ, Smits M, Kros JM et al (2017) Diffuse infiltrating oligodendroglioma and astrocytoma. J Clin Oncol 35(21):JCO2017726737

18. Jenkinson MD, Du PD, Smith TS et al (2006) Histological growth patterns and genotype in oligodendroglial tumours: correlation with MRI features. Brain 129(Pt 7):1884

19. Megyesi JF, Kachur E, Lee DH et al (2004) Imaging correlates of molecular signatures in oligodendrogliomas. Clin Cancer Res 10:4303–4306

20. Patel SH, Poisson LM, Brat DJ et al (2017) T2-FLAIR mismatch, an imaging biomarker for IDH and 1p/19q status in lower grade gliomas: a TCGA/TCIA project. Clin Cancer Res. https://doi.org/10.1158/1078-0432.CCR-17-0560

21. Mpg B, Smits M, Mmj W et al (2018) The T2-FLAIR mismatch sign as an imaging marker for non-enhancing IDH-mutant, 1p/19q-intact lower grade glioma: a validation study. Neuro Oncol. https://doi.org/10.1093/neuonc/noy048

22. Lambin P, Rios-Velazquez E, Leijenaar R et al (2012) Radiomics: extracting more information from medical images using advanced feature analysis. Eur J Cancer 48:441–446

23. Kumar V, Gu Y, Basu S et al (2012) Radiomics: the process and the challenges. Magn Reson Imaging 30:1234–1248

24. Zhou M, Hall L, Goldgof D et al (2014) Radiologically defined ecological dynamics and clinical outcomes in glioblastoma multiforme: preliminary results. Transl Oncol 7:5–13

25. Zhou M, Scott J, Chaudhury B et al (2017) Radiomics in brain tumor: image assessment, quantitative feature descriptors, and machine-learning approaches. Am J Neuroradiol 39(12):208–216

26. Zhou M, Chaudhury B, Hall LO et al (2017) Identifying spatial imaging biomarkers of glioblastoma multiforme for survival group prediction. J Magn Reson Imaging 46(1):115–123

27. Aerts HJWL, Velazquez ER, Leijenaar RTH et al (2014) Decoding tumour phenotype by noninvasive imaging using a quantitative radiomics approach. Nat Commun 5:4006

28. Huang YQ, Liu ZY et al (2016) Radiomics signature: a potential biomarker for the prediction of disease-free survival in early-stage (I or II) non-small cell lung cancer. Radiology 281(3):947

29. Huang YQ, Liang CH, He L et al (2016) Development and validation of a radiomics nomogram for preoperative prediction of lymph node metastasis in colorectal cancer. J Clin Oncol 34:2157–2164

30. Henson JW, Gaviani P, Gonzalez RG (2005) MRI in treatment of adult gliomas. Lancet Oncol 6:167–175

31. Yushkevich PA, Piven J, Hazlett HC et al (2006) User-guided 3D active contour segmentation of anatomical structures: significantly improved efficiency and reliability. Neuroimage 31:1116–1128

32. Gebejes A, Huertas R (2013) Texture characterization based on grey-level co-occurrence matrix. Proc Conf Inf Manag Sci 2:375–378

33. Galloway MM (1975) Texture analysis using gray level run lengths. Comput Graph Image Process 4:172–179

34. Chu A, Sehgal CM, Greenleaf JF (1990) Use of gray value distribution of run lengths for texture analysis. Pattern Recognit Lett 11:415–419

35. Dasarathy BV, Holder EB (1991) Image characterizations based on joint gray level run length distributions. Pattern Recognit Lett 12:497–502

36. Thibault G, Fertil B, Navarro C et al (2013) Shape and texture indexes application to cell nuclei classification. Int J Pattern Recognit Artif Intell 27:1357002

37. Amadasun M, King R (1989) Textural features corresponding to textural properties. IEEE Trans Syst Man Cybern 19:1264–1274

38. Kim SH, Kim H, Kim TS (2005) Clinical, histological, and immunohistochemical features predicting 1p/19q loss of heterozygosity in oligodendroglial tumors. Acta Neuropathol 110:27–38

39. DeLong ER, DeLong DM, Clarke-Pearson DL (1988) Comparing the areas under two or more correlated receiver operating characteristic curves: a nonparametric approach. Biometrics 44:837–845

40. Louis BN, Jana P, Joachim B et al (2018) NCCN Guidelines Version 1.2018 Panel Members Central Nervous System Cancers. National Comprehensive Cancer Network

41. Buckner J, Giannini C, Eckelpassow J et al (2017) Management of diffuse low-grade gliomas in adults - use of molecular diagnostics. Nat Rev Neurol 13(6):340–351

42. Chahlavi A, Kanner A, Peereboom D et al (2003) Impact of chromosome 1p status in response of oligodendroglioma to temozolomide: preliminary results. J Neurooncol 61:267–273

43. Alattar AA, Brandel MG, Hirshman BR et al (2017) Oligodendroglioma resection: a surveillance, epidemiology, and end results (SEER) analysis. J Neurosurg 128:1076–1083

44. Yang XF et al (2012) Ultrasound GLCM texture analysis of radiation-induced parotid-gland injury in head-and-neck cancer radiotherapy: an in vivo study of late toxicity. Med Phys 39(9):5732

45. Brown R, Zlatescu M, Sijben A et al (2008) The use of magnetic resonance imaging to noninvasively detect genetic signatures in oligodendroglioma. Clin Cancer Res 14:2357–2362

46. Sanai N, Chang S, Berger MS (2011) Low-grade gliomas in adults: a review. J Neurosurg 115:1–18

Affiliations

Yuqi Han[1,2,4] · Zhen Xie[3] · Yali Zang[2,4,8] · Shuaitong Zhang[2,4,8] · Dongsheng Gu[2,4,8] · Mu Zhou[5] · Olivier Gevaert[5] · Jingwei Wei[2,4,8] · Chao Li[3] · Hongyan Chen[6] · Jiang Du[6] · Zhenyu Liu[2,4,8] · Di Dong[2,4,8] · Jie Tian[2,4,7,8] · Dabiao Zhou[3,9]

1 School of Life Science and Technology, Xidian University, Xi'an 710126, China

2 Key Laboratory of Molecular Imaging, Institute of Automation, Chinese Academy of Sciences, Beijing 100190, China

3 Department of Neurosurgery, Beijing Tiantan Hospital, Capital Medical University, Beijing 100050, China

4 Beijing Key Laboratory of Molecular Imaging, Beijing 100190, China

[5] Stanford Center for Biomedical Informatics Research, Stanford University, Palo Alto, CA, USA

[6] Department of Neuroradiology, Beijing Neurosurgical Institute, Capital Medical University, No. 6 Tiantanxili, Dongcheng District, Beijing 100050, China

[7] The State Key Laboratory of Management and Control for Complex Systems, Institute of Automation, Chinese Academy of Sciences, Beijing 100190, China

[8] University of Chinese Academy of Sciences, Beijing 100049, China

[9] China National Clinical Research Center for Neurological Diseases, Beijing 100050, China